

Site M0066¹

T. Andrén, B.B. Jørgensen, C. Cotterill, S. Green, E. Andrén, J. Ash, T. Bauersachs, B. Cragg, A.-S. Fanget, A. Fehr, W. Granoszewski, J. Groeneveld, D. Hardisty, E. Herrero-Bervera, O. Hyttinen, J.B. Jensen, S. Johnson, M. Kenzler, A. Kotilainen, U. Kotthoff, I.P.G. Marshall, E. Martin, S. Obrochta, S. Passchier, N. Quintana Krupinski, N. Riedinger, C. Slomp, I. Snowball, A. Stepanova, S. Strano, A. Torti, J. Warnock, N. Xiao, and R. Zhang²

Chapter contents

Introduction	1
Operations	1
Lithostratigraphy	2
Biostratigraphy	3
Geochemistry	3
Physical properties	4
Paleomagnetism	5
Stratigraphic correlation	6
Reference	7
Figures	8
Tables	22

Introduction

During Integrated Ocean Drilling Program (IODP) Expedition 347, cores were recovered from two holes at Site M0066 (Bornholm Basin), with an average site recovery of 77.7%. The water depth was 82 m, with a tidal range of <10 cm. Existing data sets, including seismic reflection profiles, were evaluated prior to coring to attempt to guide the initial drilling with an anticipated lithologic breakdown. The total time spent on station was 0.96 days.

Operations

Transit to Hole M0066A

Following completion of Hole M0065C, it was decided that the alternate site should also be cored (1.4 km to the east) to capture the lower till stratigraphy in a location where the upper sequence was condensed, bringing the lower sequence within coring range. It was inferred from the seismic data that the stratigraphy at the alternate site consists of a shorter upper clay sequence; therefore, the target depth for holes at Site M0066 was set at 25 m. The vessel arrived on site at 0723 h on 26 October 2013, and operations commenced (Table T1).

Hole M0066A

Prior to drilling, it was necessary to conduct a camera survey over the locations for Holes M0066A and M0066B to assess the presence of any chemical contaminants at the surface. Again, additional personal protective equipment (PPE) was worn for the first run (after washing down the uppermost 2 m). The first piston corer system (PCS) core was recovered to deck at 0845 h on 26 October 2013. Coring continued throughout the day using the PCS, nonrotating core barrel (NRCB), and hammer sampler because the stratigraphy showed considerable variability between clay, sand, silt, and diamicton. The hole ended at 28.0 meters below seafloor (mbsf) following recovery of sand in Runs 19–21.

A total of 18 cores were recovered from Hole M0066A, with three further open-hole sections. Hole recovery was 76.82% when the open-hole sections were discounted.

¹Andrén, T., Jørgensen, B.B., Cotterill, C., Green, S., Andrén, E., Ash, J., Bauersachs, T., Cragg, B., Fanget, A.-S., Fehr, A., Granoszewski, W., Groeneveld, J., Hardisty, D., Herrero-Bervera, E., Hyttinen, O., Jensen, J.B., Johnson, S., Kenzler, M., Kotilainen, A., Kotthoff, U., Marshall, I.P.G., Martin, E., Obrochta, S., Passchier, S., Quintana Krupinski, N., Riedinger, N., Slomp, C., Snowball, I., Stepanova, A., Strano, S., Torti, A., Warnock, J., Xiao, N., and Zhang, R., 2015. Site M0066. In Andrén, T., Jørgensen, B.B., Cotterill, C., Green, S., and the Expedition 347 Scientists, *Proc. IODP, 347*: College Station, TX (Integrated Ocean Drilling Program).
doi:10.2204/iodp.proc.347.110.2015

²Expedition 347 Scientists' addresses.



Hole M0066B

Following completion of Hole M0066A, the vessel moved under dynamic positioning to commence operations in Hole M0066B. Additional PPE was worn for the first run, as previously detailed, following washing down of the uppermost 2 m. The aim of Hole M0066B was to achieve a composite recovery record with Hole M0066A, so specific intervals were targeted using a combination of push coring assembly, NRCB, and piston coring.

The first core was recovered at 1955 h on 26 October 2013, and coring continued to 27 October with the final core recovered at 0250 h. The vessel then prepared for transit to Site M0067.

A total of nine cores were recovered from Hole M0066B, with a further five runs drilled using the NRCB or noncoring assembly. The hole reached a maximum depth of 27.85 mbsf. Hole recovery was 78.61% when open-hole sections were discounted.

Lithostratigraphy

At Site M0066, two holes were drilled: Hole M0066A to a total depth of 28 mbsf, and Hole M0066B to a total depth of 27.85 mbsf. Open holing of the upper 2 mbsf at this site was necessary because of possible contamination with hazardous materials. Between ~2 and 15 mbsf, core recovery by piston coring was approximately 80%–85% in each of the holes. Deeper than ~15 mbsf, coring advanced using primarily the nonrotating core barrel in Hole M0066A with reduced recovery and a combination of nonrotating core barrel, push coring, and piston coring in Hole M0066B, resulting in 100% recovery in the interval between 20 and 27 mbsf (see “[Operations](#)”). In both holes, coring terminated in a massive glauconitic sand unit.

Lithostratigraphic divisions (Units I–IV; Fig. [F1](#)) are based on descriptions of the cut face of the split core and observations from smear slides (see “[Core descriptions](#)”). The stratigraphy of the upper ~9 mbsf (Unit I) shows similarities to that recovered from Sites M0064 and M0065.

Unit I

Subunit Ia

Intervals: 347-M0066A-2H-1, 0 cm, to 2H-2, 142 cm; 347-M0066B-2H-1, 0 cm, to 3H-1, 26 cm
 Depths: Hole M0066A = 2.0–4.92 mbsf; Hole M0066B = 2.0–5.56 mbsf

Subunit Ib

Intervals: 347-M0066A-2H-2, 142 cm, to 4H-1, 0 cm; 347-M0066B-3H-1, 26 cm, to 5H-1, 0 cm
 Depths: Hole M0066A = 4.92–8.6 mbsf; Hole M0066B = 5.56–9.6 mbsf

Unit I comprises dark grayish brown to dark gray laminated silty clay and silty fine sand with dispersed clasts. The clay is rhythmically laminated by color and texture on a centimeter scale, with lamina thickness decreasing downhole from 4–10 cm at the top of Subunit Ia to 2–3 cm thickness at the bottom of Subunit Ia and throughout Subunit Ib. Lamination is planar, parallel, and inclined. The grayish brown Subunit Ia is separated from the dark gray Subunit Ib by a 2–8 cm thick dark brown lamina. Color contacts between subunits are sharp and steeply inclined (Fig. [F2](#)). Dispersed gravel-sized rock clasts are present near the base of Subunit Ib.

The sediments were deposited in a glaciolacustrine depositional environment.

Unit II

Intervals: 347-M0066A-4H-1, 0 cm, to 9N-1, 0 cm; 347-M0066B-5H-1, 0 cm, to 8N-1, 0 cm
 Depths: Hole M0066A = 8.6–15.2 mbsf; Hole M0066B = 9.6–15.4 mbsf

This unit consists of grayish brown parallel-bedded massive medium sand with centimeter- to decimeter-scale laminated silt and clay interbeds. Glauconite is a common component of the sand.

This unit was probably deposited in a glaciofluvial depositional environment. The glauconite was likely reworked from local bedrock.

Unit III

Intervals: 347-M0066A-9N-1, 0 cm, to 13N-1, 81 cm; 347-M0066B-8N-1, 0 cm, to 12H-1, 0 cm
 Depths: Hole M0066A = 15.2–19.51 mbsf; Hole M0066B = 15.4–19.4 mbsf

Unit III is clast-rich muddy diamicton and clayey silt with dispersed clasts. Clast sizes are up to several centimeters with a high abundance of granule-sized clasts. Rare color banding and wispy lamination is present.

This unit represents deposition in an ice-proximal environment. The color banding, changes in clast abundance, and wispy laminations are consistent with a glaciolacustrine or glaciomarine depositional environment.

Unit IV

Intervals: 347-M0066A-13N-1, 81 cm, to end of hole; 347-M0066B-12H-1, 0 cm, to end of hole

Depths: Hole M0066A = 19.51–28.00 mbsf; Hole M0066B = 19.4–27.25 mbsf

This unit comprises parallel-bedded dark greenish gray massive medium sand. Centimeter- to decimeter-scale interbeds of clay and partly laminated silt are found interbedded with the sand. Glauconite is common in the sand fraction.

These sediments were probably deposited in a fluvial or glaciofluvial depositional environment. The glauconite could be reworked from local bedrock.

Biostratigraphy

Diatoms

Section tops from Hole M0066A were analyzed for siliceous microfossils. No siliceous microfossils were found in any of the samples analyzed.

Foraminifers and ostracods

A total of 30 samples (17 core catchers and 13 On-shore Science Party [OSP] samples) from Site M0066 were prepared for foraminiferal and ostracod analysis. Quaternary foraminifers and ostracods do not occur in the sediments sampled from this site, although some redeposited pre-Quaternary foraminifers and ostracods are present in the lower diamicton and sand units. Unlike nearby Site M0065, this site does not contain an organic-rich clay unit at the surface (which may have represented the brackish period at Site M0065). The lack of this organic-rich clay deposit and the lack of Quaternary foraminifers and ostracods suggests that the brackish unit was not recovered here, perhaps because of open holing in the upper ~2 m. Almost no microfossils >63 μm are present, even in the upper gray-brown clay (Unit 1), suggesting that this deposit may represent a low-productivity freshwater environment (see “[Lithostratigraphy](#)”).

Palynological results

Palynological analyses for this site focused on Hole M0066A. Two samples from Hole M0066A (core catcher samples from Cores 347-M006A-2H and 11H) were analyzed in total. As expected from the sedimentologic data, the samples were virtually barren of palynomorphs, probably because of oxidation of the organic material. Therefore, no palynological data could be generated for this site.

Geochemistry

Interstitial water

At Site M0066, freshwater and glaciolacustrine deposits are overlain by <2 m of brackish-marine sediment (see “[Lithostratigraphy](#)” and “[Biostratigraphy](#)”). Because of safety issues, the upper ~2 m of the sediment was not sampled (see “[Operations](#)”). The chemical composition of the pore water (Table T2) is consistent with more limited input of organic matter and lower rates of sediment accumulation when compared to the nearby Site M0065.

Salinity variations: chloride, salinity, and alkalinity

Concentrations of chloride (Cl^-) are highest near the surface at ~170 mM and then decline to ~25 mM deeper than 20 mbsf (Fig. F3A; Table T2). Pore water salinity from shipboard measurements with a refractometer and as calculated from Cl^- concentrations are in close agreement and decline with depth from ~11 to 2 (Table T2; Fig. F3B–F3C). Given the limited thickness of the brackish-marine deposit, the penetration of Cl^- into the sediment at this site largely relies on molecular diffusion. Alkalinity is relatively constant with depth at ~4 meq/L (Fig. F3D).

Organic matter degradation: sulfate, sulfide, ammonium, phosphate, and bromide

Sulfate (SO_4^{2-}) penetrates to ~10 mbsf (Fig. F4A). Methane and sulfide were not analyzed at this site. Pore water ammonium (NH_4^+) and phosphate (PO_4^{3-}) concentrations are relatively low, ~0.15 and 0.01 mM, respectively, around 3 mbsf and show only a minor but consistent decline with depth (Fig. F4B–F4C; Table T2). Dissolved iron (Fe^{2+}) and manganese (Mn^{2+}) concentrations are highest in the upper 5–10 m of the sediment, with maxima of ~140 and 40 μM , respectively (Fig. F4D–F4E). Pore water pH decreases in the upper part of the sediment and then increases and/or stays relatively constant deeper than ~10 mbsf in the different holes (Fig. F4F). Concentrations of NH_4^+ , PO_4^{3-} , and alkalinity are more than an order of magnitude lower at Site M0066 compared to Site M0065. This difference can be explained by the thinner brackish-marine deposit and associated lower rate of organic matter input and degradation at Site M0066.

The depth profile of dissolved bromide (Br^-) is similar to the Cl^- profile (Fig. F5A). The profile of Br/Cl does reveal a slight enrichment in pore water Br^- relative to Cl^- with depth (Fig. F5B; Table T3). Dis-

solved boron (B) concentrations decrease from 80 to 40 μM between 3 and 8 mbsf and stay relatively constant with depth deeper than 8 mbsf (Fig. F5C). Concentrations of boron at Site M0066 are distinctly lower than those measured at nearby Site M0065. Ratios of B/Cl increase with depth (Fig. F5D). However, given the low salinities at depth, this trend should be interpreted with caution.

Mineral reactions

Sodium, potassium, magnesium, and calcium

Profiles of sodium (Na^+), potassium (K^+), and magnesium (Mg^{2+}) are similar to those of Site M0065, but concentrations are lower and maxima are limited to a more narrow depth zone near the sediment surface (Fig. F6A–F6C). Slightly elevated concentrations of calcium (Ca^{2+}) are observed in the upper ~3–8 m of the sediment column when compared to deeper layers (Fig. F6D). Ratios of Na/Cl, K/Cl, and Mg/Cl are either at or below those for seawater, whereas those for Ca/Cl are consistently above the seawater ratio (Fig. F6E–F6H; Table T3). Given the low salinity of the pore water at this site, care should be taken in interpreting these ratios within the context of reactions.

Silica, lithium, barium, and strontium

Concentrations of dissolved silica (H_4SiO_4) and lithium (Li^+) in the pore water are largely constant with depth and vary around 400 and 10 μM , respectively (Fig. F7A–F7B). Concentrations of barium (Ba^{2+}) are generally low ($<2 \mu\text{M}$) but show a gradual increase with depth (Fig. F7C). Pore water strontium (Sr^{2+}) concentrations slightly decrease with depth from ~40 to 27 μM (Fig. F7D). The contrasting results for Site M0066 compared to Site M0065 indicate differences in mineral reactions linked to differences in salinity and organic matter input.

Sediment

Carbon content

The total carbon (TC) content at Site M0066 varies between 0.6 and 3.2 wt% with maxima around 6 mbsf and between 17 and 20 mbsf (Fig. F8A; Table T4). The total organic carbon (TOC) content is generally low, with values ranging from 0.01 to 0.54 wt% and highest values observed at the core top (Fig. F8B). A second maximum with TOC values of up to 0.3 wt% is present in an interval from 16 to 22 mbsf. Note that any brackish-marine sediment that may have been present in the uppermost 2 m of the investigated profile was not sampled.

The total inorganic carbon content (TIC) varies from 0.5 to 3.0 wt% (Fig. F8C; Table T4), indicating that

the major part of the carbon at Site M0066 is present in inorganic form. Similar to the TC profile, two maxima in TIC are observed at 6 mbsf and between 16 and 22 mbsf. Deeper than 22 mbsf, the TIC content gradually declines to values around 1 wt% close to the base of the investigated profile.

Sulfur content

The total sulfur (TS) content ranges from 0.1 to 0.7 wt% and shows a trend of increasing values with depth. Between 18 and 21 mbsf, TS values reach a maximum of 0.7 wt% (Fig. F8D; Table T4). Note that this maximum in sulfur content roughly correlates with that in TOC content, suggesting that sulfur in the deeper sediment may be largely incorporated in organic matter.

Physical properties

This section summarizes the preliminary results from Site M0066. Two holes were drilled at Site M0066. Hole M0066A was drilled to 28.00 mbsf, and Hole M0066B was drilled to 27.85 mbsf. For each hole, the uppermost 2 m was washed down because of potential contamination from hazardous materials. Despite $<100\%$ recovery, sediments recovered from Hole M0066A provide a more continuous and better record of the physical properties at Site M0066. For Hole M0066A, all physical property measurements described in “Physical properties” in the “Methods” chapter (Andrén et al., 2015) were conducted. As the thermal conductivity data and the discrete moisture and density (MAD) and *P*-wave measurements are few in number, the interpretations are based primarily on the shipboard multisensor core logger (MSCL) data and natural gamma ray (NGR) data.

Natural gamma radiation

High-resolution NGR exhibits relatively constant values (~10 cps) in lithostratigraphic Subunit Ia (Fig. F9). From ~5 to 8 mbsf, throughout lithostratigraphic Subunit Ib, NGR shows generally decreasing values (from ~10 to 6 cps). At the Subunit Ib/Unit II boundary, a shift to lower values (~5 cps) is observed. NGR exhibits generally low (<5 cps) and variable values in lithostratigraphic Unit II. Negative excursions potentially reflect an increase in silt or sand content, whereas positive excursions may result from an increase in clay or glauconite content (see “Lithostratigraphy”). At the Unit II/III boundary (~15.7 mbsf), NGR increases to >10 cps and, though recovery is moderate, these high values appear consistent throughout lithostratigraphic Unit III. This change could be related to an increase in clay content within lithostratigraphic Unit III (see “Lithostratigraphy”).

NGR exhibits an overall decreasing trend toward the base of lithostratigraphic Unit IV (from ~13 to 5 cps), which is interpreted to result from an increased silt and sand content in lithostratigraphic Unit IV (see “**Lithostratigraphy**”).

Shipboard magnetic susceptibility and noncontact resistivity

Magnetic susceptibility shows low ($\sim 15 \times 10^{-5}$ SI) and constant values in lithostratigraphic Subunit Ia (Fig. F9). Near the Subunit Ia/Ib boundary, magnetic susceptibility increases to $\sim 40 \times 10^{-5}$ SI and remains high through lithostratigraphic Subunit Ib. At the Subunit Ib/Unit II boundary, magnetic susceptibility values decrease sharply ($< 5 \times 10^{-5}$ SI) and maintain a low mean to ~12 mbsf, with the exception of two positive excursions. Magnetic susceptibility increases strongly from ~12 to 13.5 mbsf, and an abrupt spike that could reflect a change in lithology ($\sim 85 \times 10^{-5}$ SI) is observed at ~14 mbsf. This dramatic increase in magnetic susceptibility coincides with a small decrease in dry density at the same depth and may be characterized as a massive sand with noted clay and fine-silt interbeds (see “**Lithostratigraphy**”). Magnetic susceptibility shows a general decreasing trend in lithostratigraphic Unit III and in the upper interval of lithostratigraphic Unit IV (from ~19.5 to 22 mbsf). Magnetic susceptibility values are low ($< 20 \times 10^{-5}$ SI) and highly variable in the lower interval of lithostratigraphic Unit IV.

Noncontact resistivity (NCR) shows an overall similar trend to magnetic susceptibility (Fig. F9). NCR values are low in lithostratigraphic Unit I, increase to ~6.5 Ωm at 8.4 mbsf, and remain constant for the majority of lithostratigraphic Unit II. NCR data are difficult to interpret within lithostratigraphic Units III and IV because of poor recovery and high variability. The upper sections of cores in these units exhibit much lower values than deeper sections of the same cores.

Density

Dry density derived from moisture and density measurements is low in lithostratigraphic Subunit Ia ($< 1 \text{ g/cm}^3$) and increases markedly in Subunit Ib to $\sim 2 \text{ g/cm}^3$ (Fig. F9). From 11.5 to 15.7 mbsf in the lower interval of lithostratigraphic Unit II, dry density decreases to $\sim 1.6 \text{ g/cm}^3$ before increasing to $\sim 2.1 \text{ g/cm}^3$ at the lithostratigraphic Unit II/III boundary. Deeper than this, density decreases toward the bottom of the hole.

Gamma density was measured at a 2 cm interval during the offshore phase of Expedition 347 (Fig.

F10). Gamma density shows relatively low values ($\sim 1.6 \text{ g/cm}^3$) through most of lithostratigraphic Subunit Ia. Gamma density exhibits a dramatic shift to higher values at the Subunit Ia/Ib boundary and remains generally high ($\sim 2 \text{ g/cm}^3$) throughout lithostratigraphic Units II, III, and IV. Discrete bulk density measurements conducted during the OSP correlate moderately well with the shipboard measurements ($r^2 = 0.46$, Fig. F10).

Paleomagnetism

To achieve the main objectives of the OSP paleomagnetic work we carried out basic analyses of the natural remanent magnetization (NRM) and ascertained the magnetic susceptibility of discrete specimens of known volume and mass (see “**Paleomagnetism**” in the “Methods” chapter [Andrén et al., 2015]). A total of 87 discrete samples were taken from Holes M0066A (17 discrete $2 \text{ cm} \times 2 \text{ cm} \times 2 \text{ cm}$ cubes and 24 discrete $1 \text{ cm} \times 1 \text{ cm} \times 1 \text{ cm}$ minicubes) and M0066B (27 discrete $2 \text{ cm} \times 2 \text{ cm} \times 2 \text{ cm}$ cubes and 19 discrete $1 \text{ cm} \times 1 \text{ cm} \times 1 \text{ cm}$ minicubes) according to the site splice, with a higher density of samples taken between 6 and 2 mbsf. Magnetic susceptibility ranges between $\sim 0.03 \times 10^{-6}$ and $0.6 \times 10^{-6} \text{ m}^3/\text{kg}$ through the sequence, with the highest value found within the lower part of Unit II (medium sand with laminated silt and clay interbeds).

The paleomagnetic pilot samples that were recovered from Unit IV (parallel-bedded dark greenish gray massive medium sand) contain a medium to hard coercivity magnetic assemblage with ~30% of the NRM intensity remaining after the 80 mT demagnetization level. Unit III samples were more easily demagnetized, almost completely demagnetized by a 80 mT alternating field (AF). Units II and I contained weak and unstable remanent magnetizations.

Discrete sample measurements

A total of 87 discrete samples were obtained from Holes M0066A and M0066B. Samples were recovered at intervals of ~25 cm (1 cm^3 minicubes) and 50 cm (standard $2 \text{ cm} \times 2 \text{ cm} \times 2 \text{ cm}$ IODP cubes) from within the site splice.

Magnetic susceptibility

The results of the magnetic analyses are shown in Figure F11. Magnetic susceptibility (χ) normalized to sample mass ranges between $\sim 0.03 \times 10^{-6}$ and $0.6 \times 10^{-6} \text{ m}^3/\text{kg}$. Samples taken from Units IV and III have χ values $< 0.3 \times 10^{-6} \text{ m}^3/\text{kg}$. Overlying Unit II has χ values that reach $0.6 \times 10^{-6} \text{ m}^3/\text{kg}$. Subunit Ib has χ values that range between 0.1×10^{-6} and 0.6×10^{-6}

m^3/kg . Subunit Ia has consistently low values of $0.1 \times 10^{-6} \text{ m}^3/\text{kg}$.

The biplots show no relationships between χ , sediment wet density, NRM intensity, and inclination.

Natural remanent magnetization and its stability

Results of the pilot sample demagnetization (Fig. F12) indicate that a low AF of 5 mT was sufficient to remove a weak viscous remanent magnetization (VRM). Three different responses to the sequential AF demagnetization are displayed by samples from Site M0066. Category 1 includes the samples from the coarse-grained sands in Units IV and II; such samples lose 50% of their NRM intensity at alternating fields of 50 mT with a residual component left at 80 mT that requires stronger fields to completely remove it even though the univectorial trend is toward the origin of the diagram. The NRM of these samples is carried by a phase with relatively high coercivity. Category 2, which includes samples in Unit III, is typified by a paleomagnetic vector that is smoothly demagnetized up to the maximum AF demagnetization level of 80 mT, with a vector that trends toward the origin of the orthogonal projection, with medium to low coercivity. Category 3 is typical of unstable magnetic remanence and is characterized by the removal of a significant viscous remanence at the 5 mT demagnetization level but displays erratic magnetic behavior at higher levels of demagnetization.

After removal of the viscous overprint the NRM intensity of the samples recovered from Site M0066 lies predominantly in the range between 0.1×10^{-3} and $20 \times 10^{-3} \text{ A/m}$ with one outlier from Unit IV at $90 \times 10^{-3} \text{ A/m}$, and there is no general positive relationship with χ (Fig. F11).

Paleomagnetic directions

The directions of the paleomagnetic vectors are illustrated by the inclination data in Figure F11. The inclination data from all units are scattered, with the majority of the inclination values on the positive side of the diagram and ~10% of inclinations on the negative side. Very few samples from these units have inclinations that approach the geocentric axial dipole (GAD) prediction for this site location. It is notable that the samples taken from Units IV, III, and II and Subunit Ib that have high χ values and relatively low NRM/ χ plot relatively far away from the GAD prediction, with a large degree of dispersion of the inclination values. We conclude that the vari-

able magnetic properties and scattered inclination data from this site preclude using the paleomagnetic data for relative dating purposes.

Stratigraphic correlation

Two holes were drilled at Site M0066: Holes M0066A (28 mbsf) and M0066B (27.25 mbsf). The meters composite depth (mcd) scale for Site M0066 was based on correlation of magnetic susceptibility between holes (Fig. F13). Sediment cores were logged with the standard MSCL to enable precise hole-to-hole correlation and to construct a composite section for Site M0066 (Fig. F13). Before analysis, all magnetic susceptibility data were cleaned from the top of each section, removing any outliers from the measurements. The depth offsets that define the composite section for Site M0066 are given in Table T5 (affine table).

Correlation between the susceptibility data in Holes M0066A and M0066B is relatively good between 2 and 15 mbsf, enabling the production of a continuous splice record for this site (Table T6). However, there are some gaps in the splice record, as Section 347-M0066B-2H-3 was appended to Section 347-M0066B-3H-1 and Section 347-M0066A-3H-2 was appended to Section 347-M0066A-4H-1. Correlation and therefore splicing was not possible deeper than Cores 347-M0066A-6H and 347-M0066B-7H. The lowermost part of Hole M0066A was therefore appended in the splice record. The accuracy of the correlation was visually checked from scanned core slab images using Corelyzer software. No expansion or compression corrections were applied to the data, so the offset within each core was equal for all points. Therefore, it is possible that some features are not similarly aligned between holes.

Seismic units

Seismic sequence boundary-sediment core-MSCL log (magnetic susceptibility) correlations are shown in Figure F14. The correlation is based on the integration of seismic data and lithostratigraphy. Two-way traveltimes were calculated for each lithostratigraphic unit boundary using sound velocity values measured during the OSP (see “Physical properties”; Table T7). Lithostratigraphic units/unit boundaries (see “Lithostratigraphy”) were examined at these calculated two-way traveltimes to define the extent of agreements between seismic boundaries and actual lithologic and/or physical properties disconformable surfaces. Uncertainties in the time-depth function and effects from gas-saturated sedi-

ments could have resulted in moderate inconsistencies between seismic features and sedimentological observations from cores and MSCL logs.

Seismic Unit I

Seismic Subunit Ia

Two-way traveltime: 0.118 ms

Lithology: laminated silty clay and silty fine sand (lithostratigraphic Subunit Ia)

Depths: 2.0–4.92 mbsf (M0066A); 2.0–5.56 mbsf (M0066B)

Subunit Ia corresponds to a relatively strong reflector in the upper part of the seismic profile. Magnetic susceptibility values are low in this unit, but they increase downcore at the Subunit Ia/Ib boundary (see “[Physical properties](#)”).

Seismic Subunit Ib

Two-way traveltime: 0.122 ms

Lithology: laminated silty clay and silty fine sand with dispersed clasts (lithostratigraphic Subunit Ib)

Depths: 4.92–8.60 mbsf (M0066A); 5.56–9.60 mbsf (M0066B)

Subunit Ib is characterized by relatively high magnetic susceptibility values and parallel reflectors in the seismic profile.

Seismic Unit II

Two-way traveltime: 0.130 ms

Lithology: parallel bedded massive medium sand with centimeter- to decimeter-scale laminated silt and clay interbeds (lithostratigraphic Unit II)

Depths: 8.6–15.2 mbsf (M0066A); 9.6–15.4 mbsf (M0066B)

The boundary between Subunit Ib and Unit II coincides with a strong reflector in the seismic profile. Magnetic susceptibility values are low at the top of Unit II but increase downcore and are highest in the lowermost part of the unit.

Seismic Unit III

Two-way traveltime: 0.135 ms

Lithology: clast-rich muddy diamicton and clayey silt with dispersed clasts (lithostratigraphic Unit III)

Depths: 15.2–19.51 mbsf (M0066A); 15.4–19.4 mbsf (M0066B)

Unit III is characterized by high magnetic susceptibility values that decrease downcore. Parallel reflectors are visible in the seismic profile.

Seismic Unit IV

Two-way traveltime: 0.147 ms

Lithology: parallel-bedded dark greenish gray massive medium sand (lithostratigraphic Unit IV).

Depths: 19.51–28.00 mbsf (M0066A); 19.4–27.25 mbsf (M0066B)

Unit IV possibly corresponds to strong parallel reflectors visible in the seismic profile. The boundary between Unit III and Unit IV coincides with a strong reflector, indicating a probable unconformity/erosion. Magnetic susceptibility values of this unit are again relatively low.

Reference

Andrén, T., Jørgensen, B.B., Cotterill, C., Green, S., Andrén, E., Ash, J., Bauersachs, T., Cragg, B., Fanget, A.-S., Fehr, A., Granoszewski, W., Groeneveld, J., Hardisty, D., Herrero-Bervera, E., Hyttinen, O., Jensen, J.B., Johnson, S., Kenzler, M., Kotilainen, A., Kotthoff, U., Marshall, I.P.G., Martin, E., Obrochta, S., Passchier, S., Quintana Krupinski, N., Riedinger, N., Slomp, C., Snowball, I., Stanova, A., Strano, S., Torti, A., Warnock, J., Xiao, N., and Zhang, R., 2015. Methods. *In* Andrén, T., Jørgensen, B.B., Cotterill, C., Green, S., and the Expedition 347 Scientists, *Proc. IODP, 347*: College Station, TX (Integrated Ocean Drilling Program). [doi:10.2204/iodp.proc.347.102.2015](https://doi.org/10.2204/iodp.proc.347.102.2015)

Publication: 20 February 2015
MS 347-110

Figure F1. Graphic lithology log summary, Site M0066. All depths referred to in the figure represent the lithostratigraphic boundaries observed in Hole M0066A.

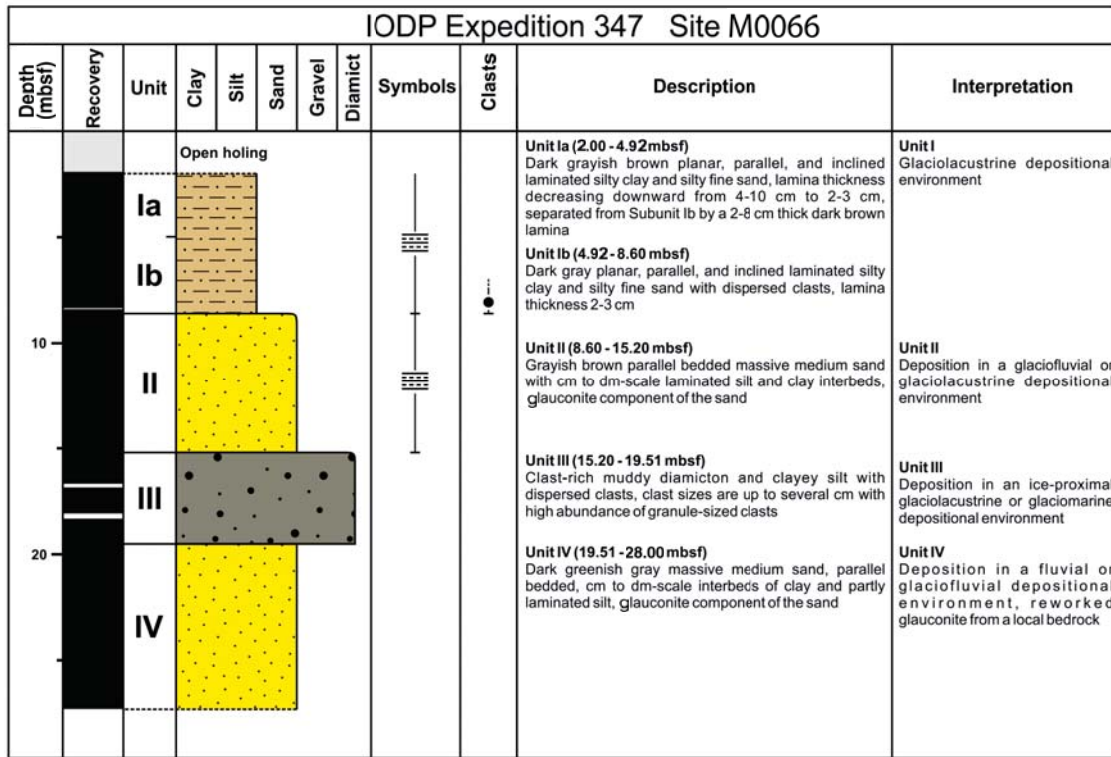


Figure F2. Color changes between Subunits Ia and Ib (interval 347-M0066B-3H-1, 12–47 cm).





Figure F3. Concentrations of (A) chloride, (B) salinity by refractometer, (C) chloride-based salinity, and (D) alkalinity in interstitial water samples, Site M0066.

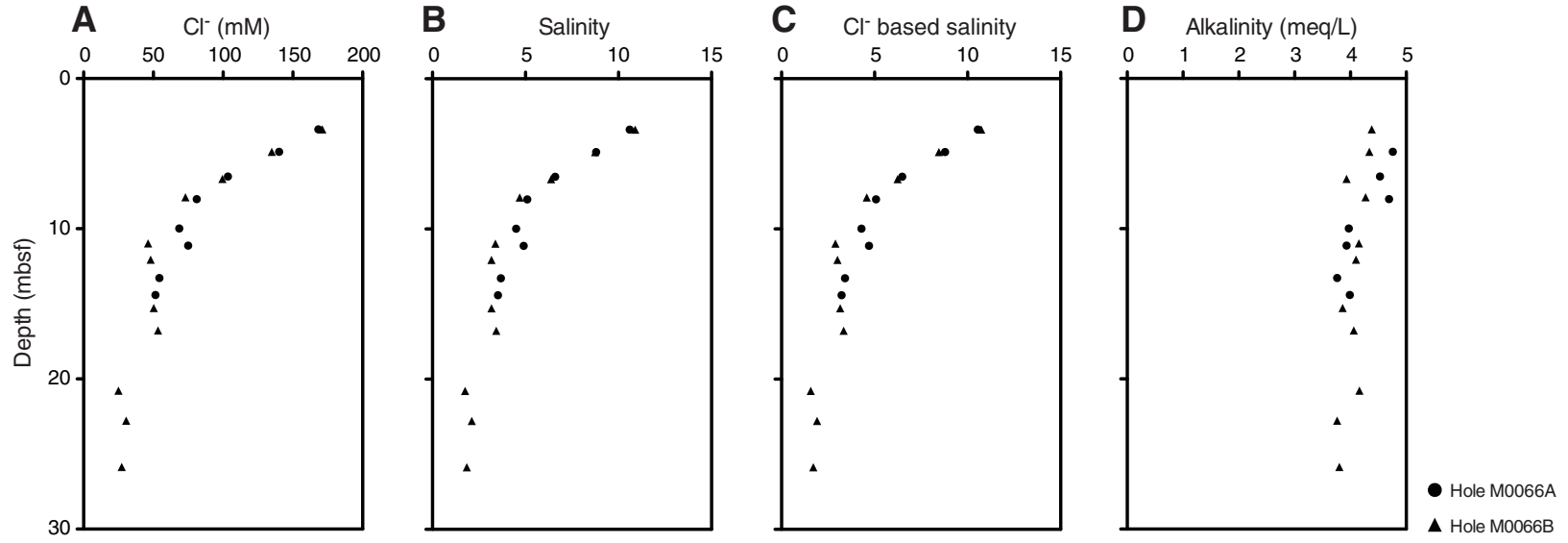




Figure F4. Concentrations of (A) sulfate, (B) ammonium, (C) phosphate, (D) iron, (E) manganese, and (F) pH from interstitial water samples, Site M0066.

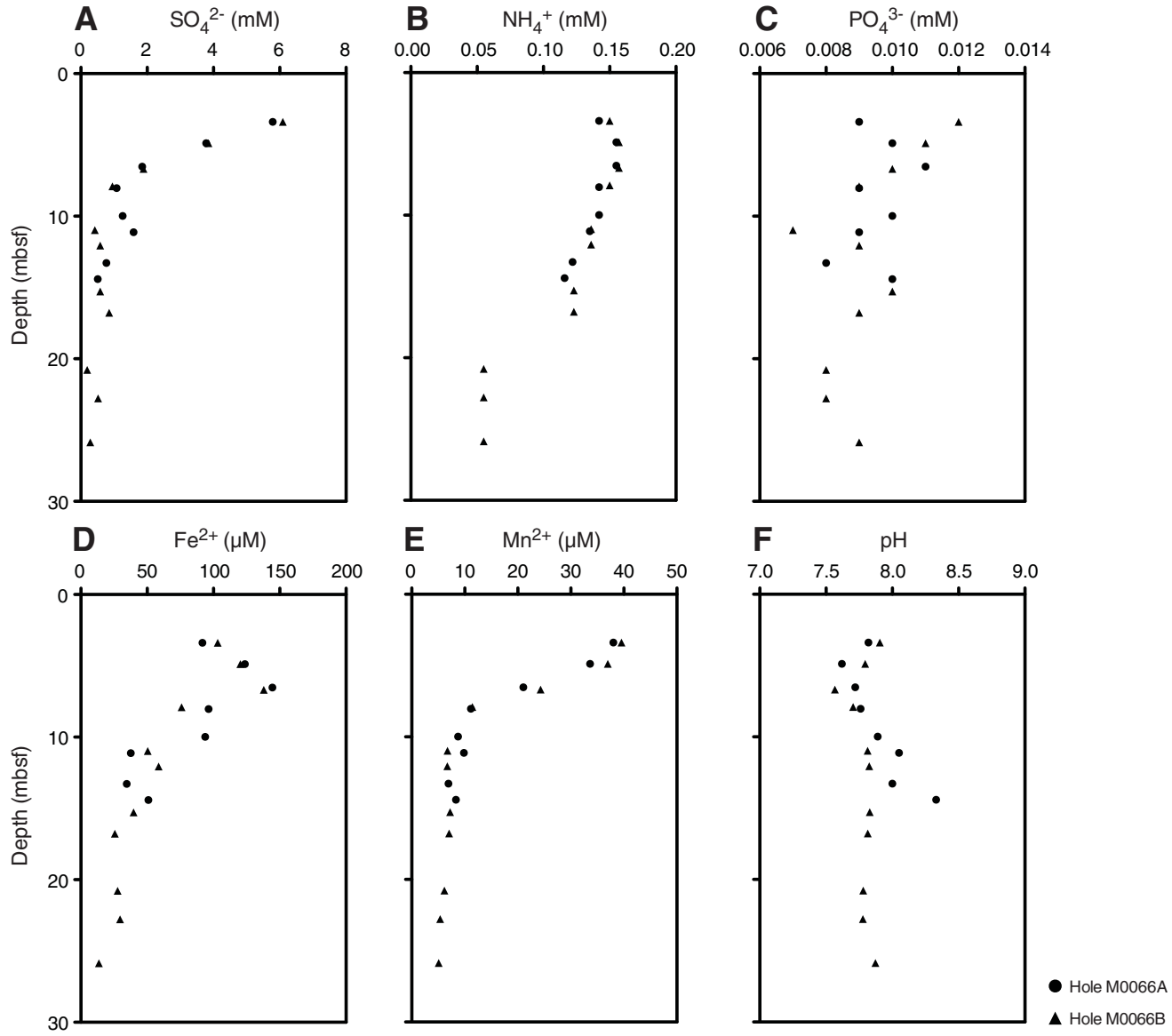




Figure F5. Concentrations and ratios of (A) bromide, (B) bromide/chloride, (C) boron, and (D) boron/chloride from interstitial waters samples, Site M0066. Dashed lines = seawater ratio.

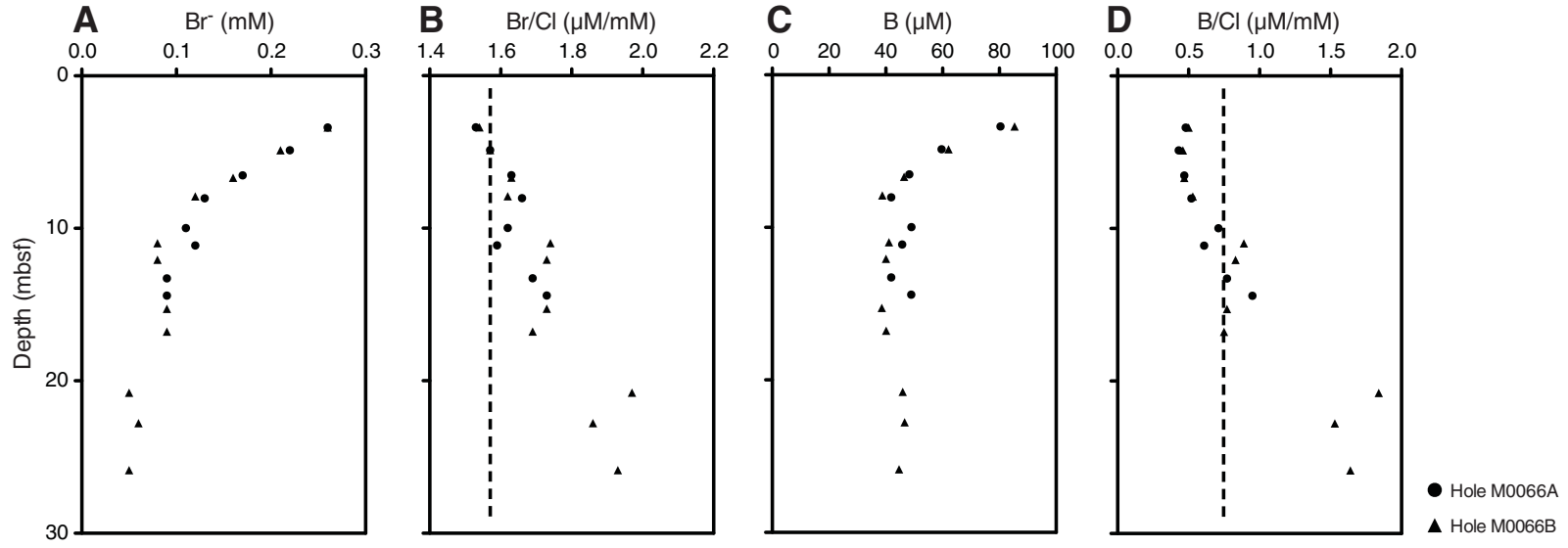


Figure F6. Concentrations and ratios of (A) sodium, (B) potassium, (C) magnesium, (D) calcium, (E) sodium/chloride, (F) potassium/chloride, (G) magnesium/chloride, and (H) calcium/chloride from interstitial waters samples, Site M0066. Dashed lines = seawater ratio.

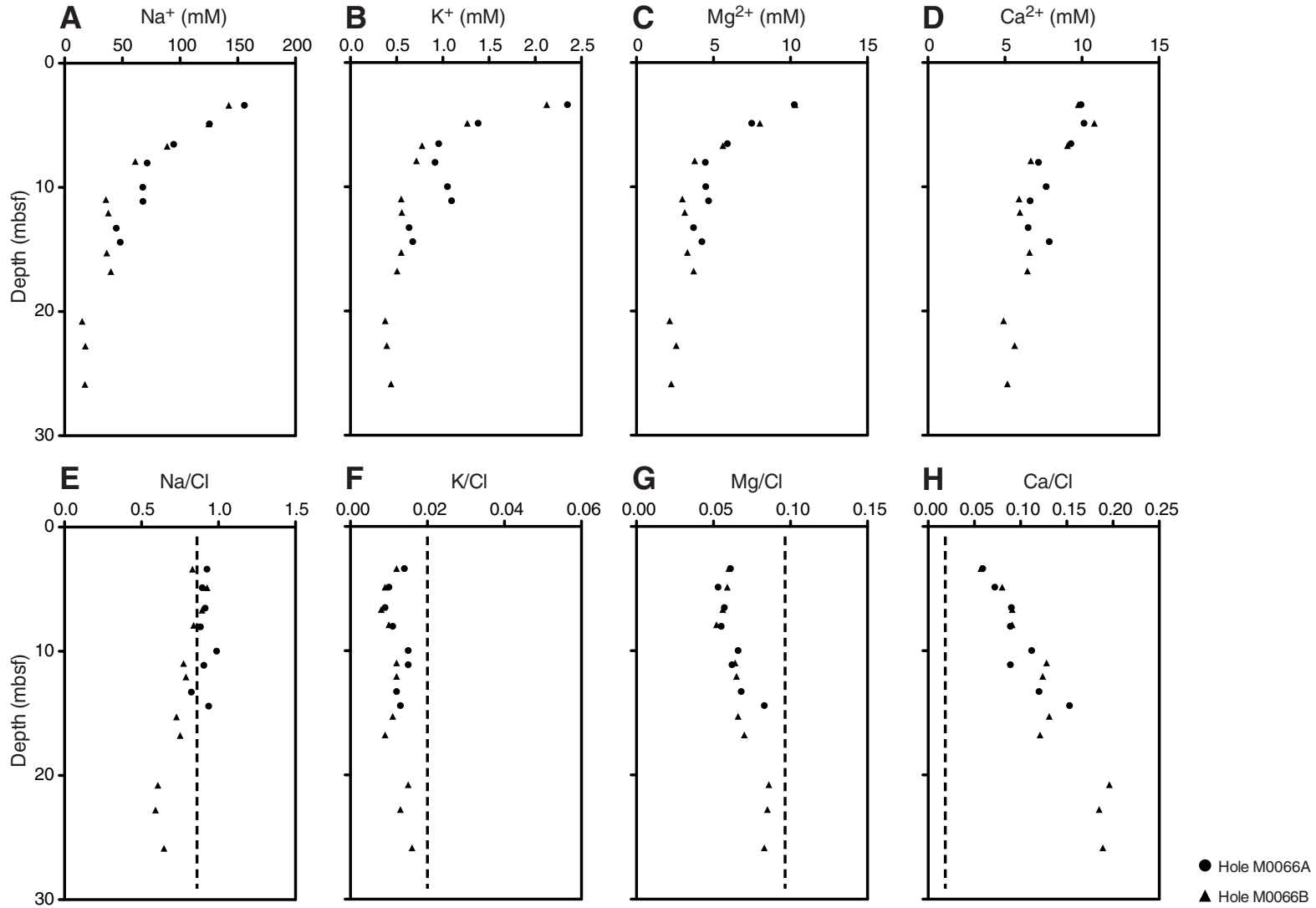




Figure F7. Concentrations of (A) dissolved silica, (B) lithium, (C) barium, and (D) strontium from interstitial water samples, Site M0066.

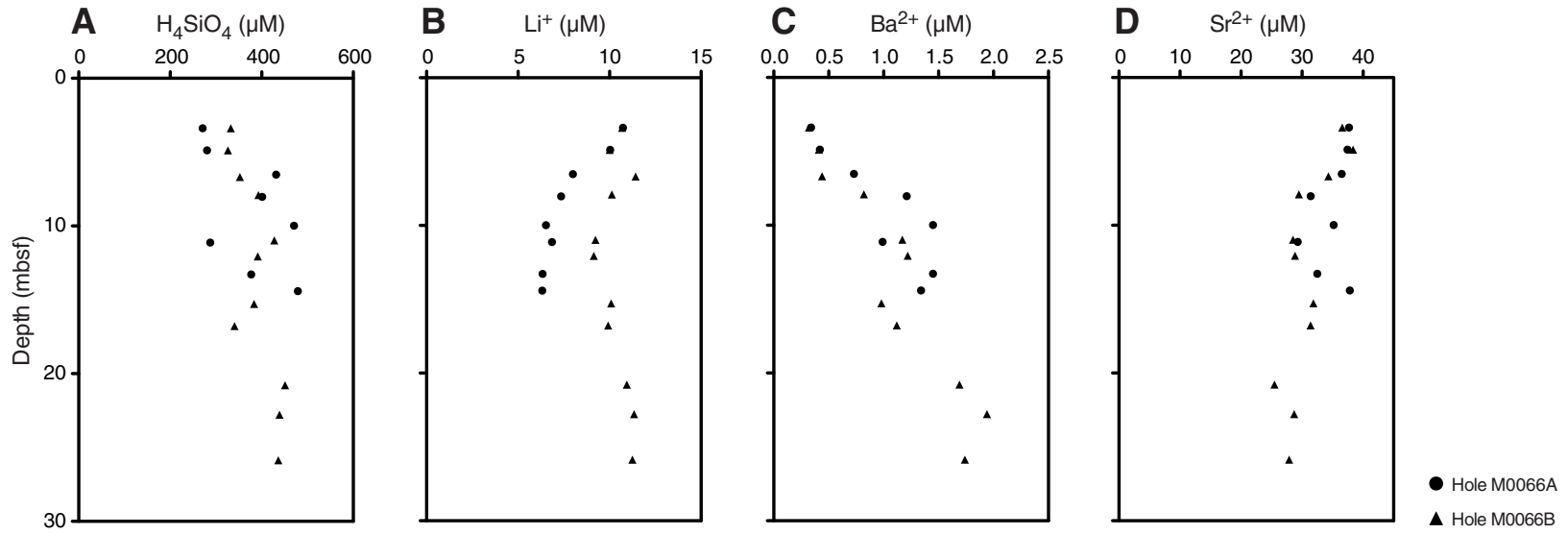




Figure F8. Sedimentary (A) total carbon (TC), (B) total organic carbon (TOC), (C) total inorganic carbon (TIC), and (D) total sulfur (TS) values, Site M0066.

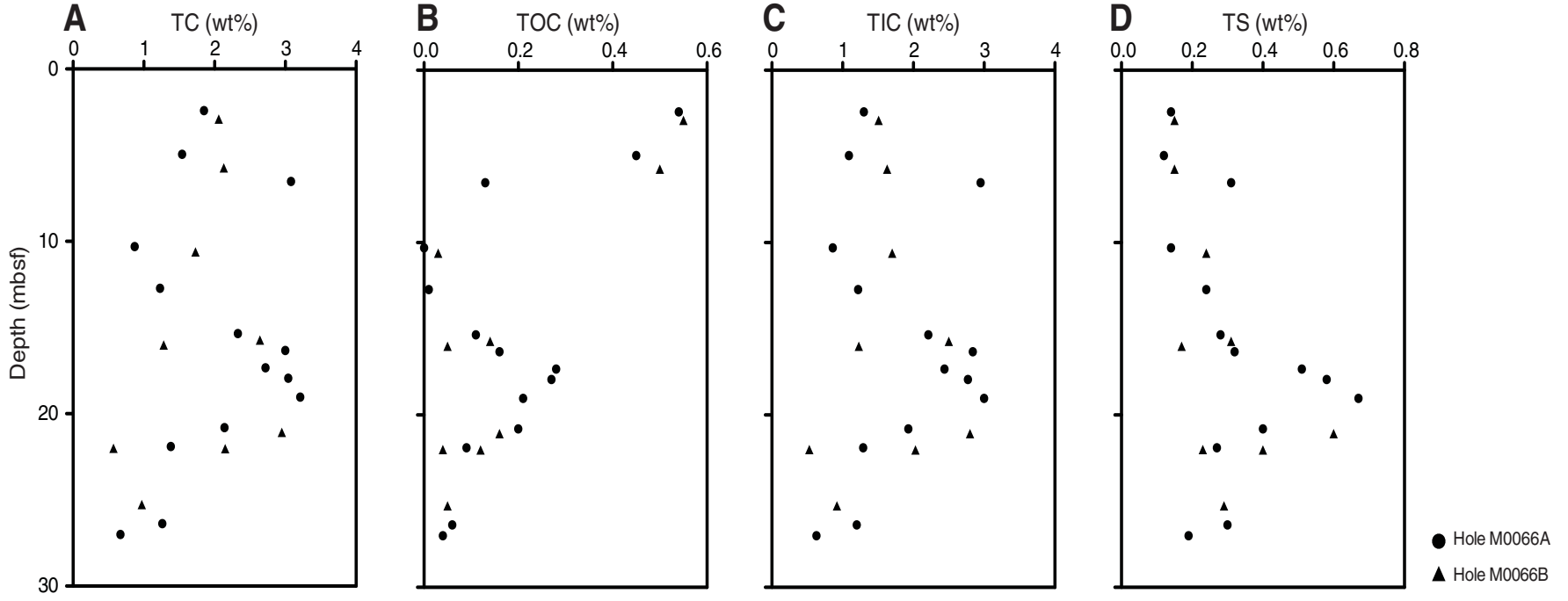


Figure F9. Natural gamma radiation (NGR) (cps), MSCL magnetic susceptibility (MS) (10^{-5} SI), MSCL non-contact resistivity (NCR) (Ωm), and dry density (g/cm^3), Hole M0066A.

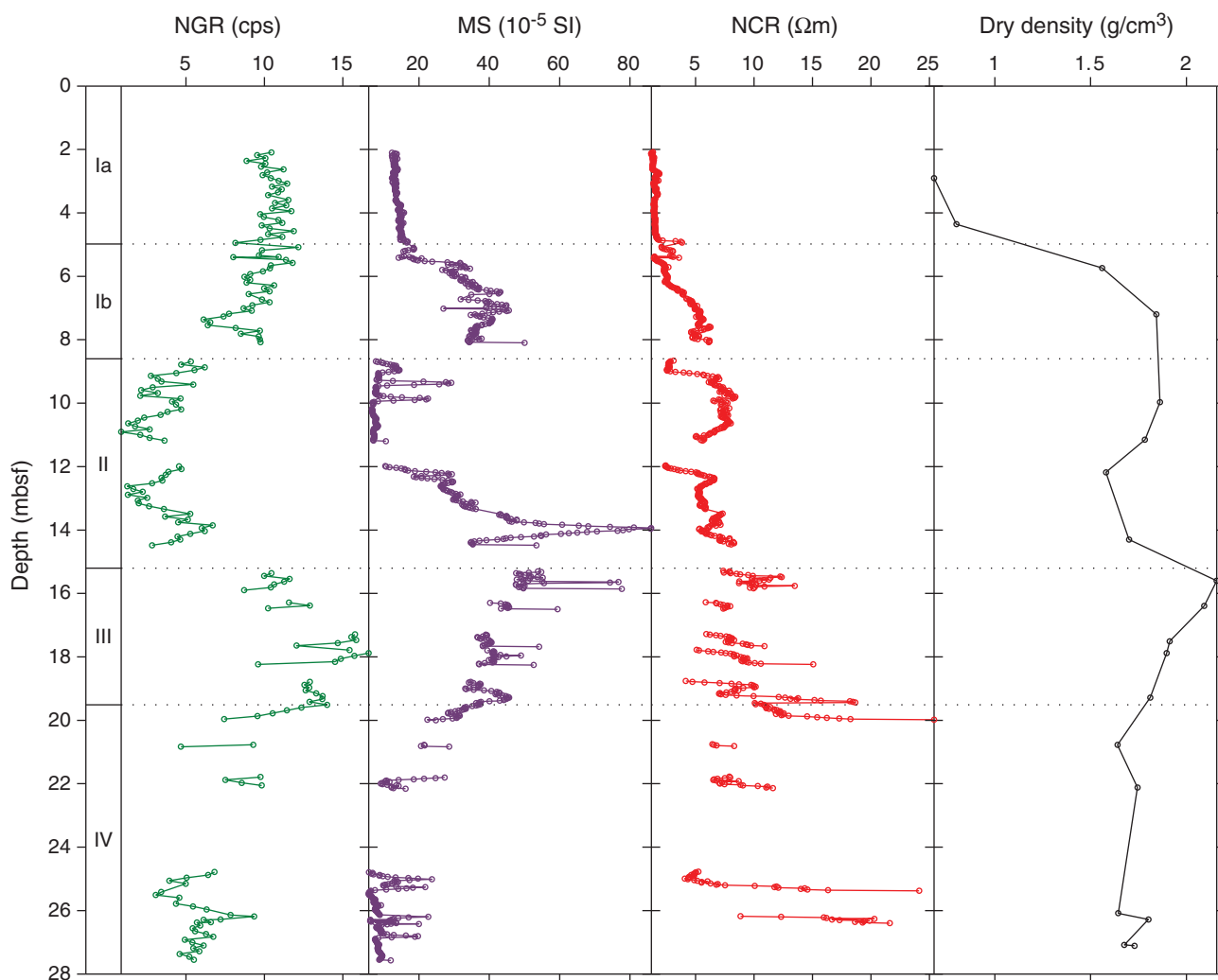


Figure F10. Gamma density (g/cm^3) and discrete bulk density (g/cm^3) measurements derived from pycnometer moisture and density analyses, Hole M0066A.

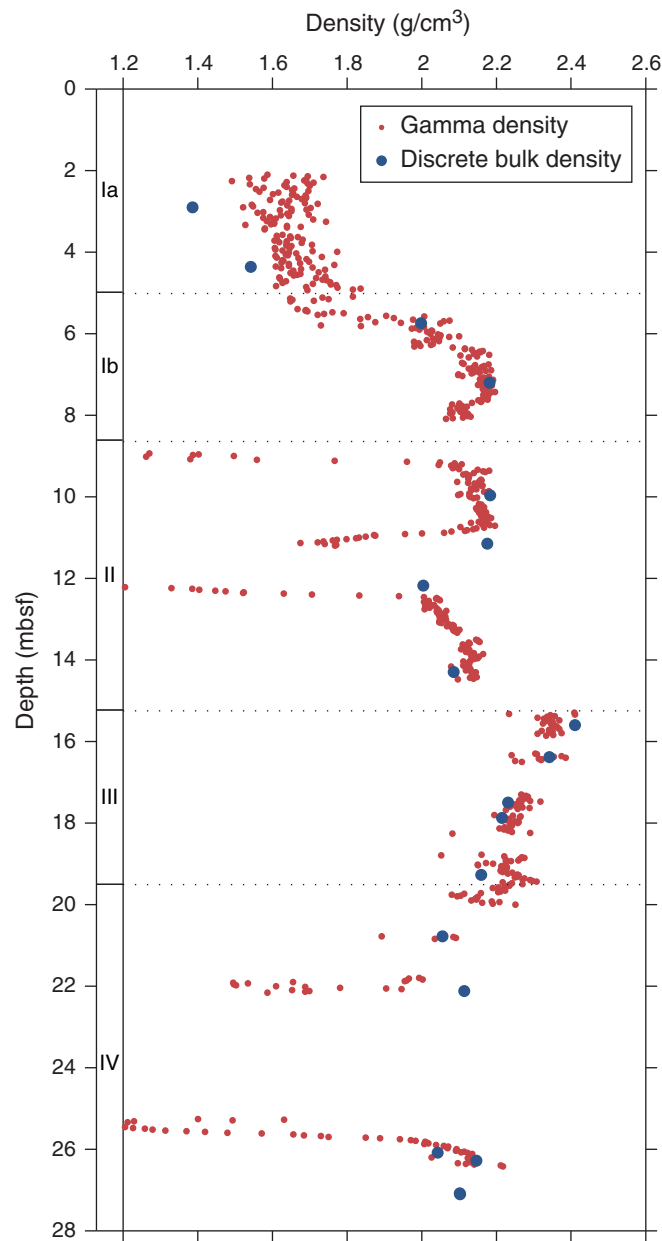




Figure F11. Plots and biplots of magnetic susceptibility (χ), natural remanent magnetization (NRM) intensity, and NRM inclination of discrete paleomagnetic samples, Holes M0066A and M0066B. Dashed line = geocentric axial dipole (GAD) prediction of inclination for the site latitude. AF = alternating field.

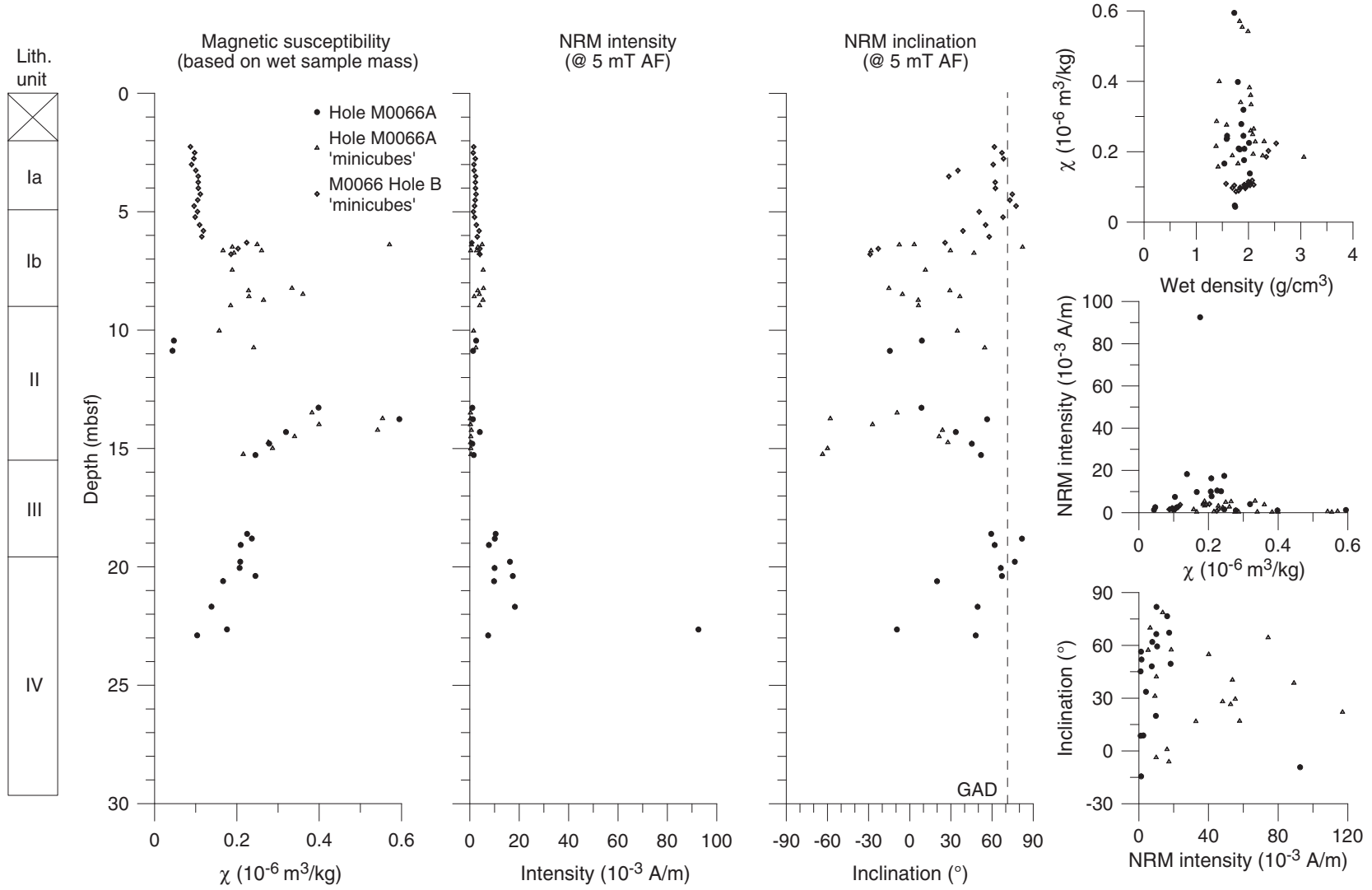


Figure F12. Plots of natural remanent magnetization (NRM) after AF demagnetization to 80 mT **A.** Sample 347-M0066A-6H-2, 6 cm; 7.47 mbsf. **B.** Sample 347-M0066A-12H-1, 53 cm; 19.07 mbsf. **C.** Sample 347-M0066A-15H-1, 14 cm; 21.68 mbsf. Category 1 and 2 vectors trend toward the origin and show good stability, whereas the Category 3 vector is characterized by poor magnetic stability. Open squares = vertical, solid squares = horizontal.

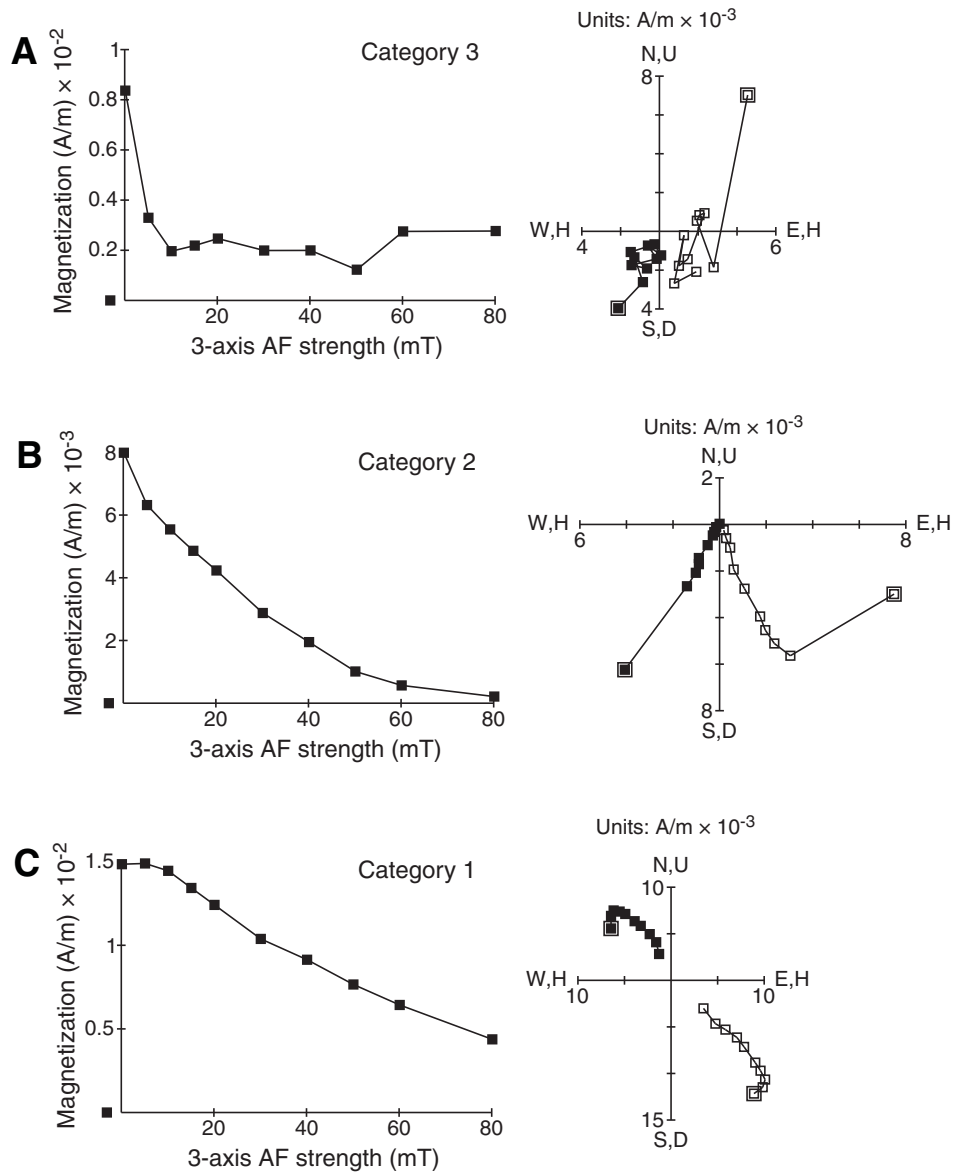


Figure F13. Plot of magnetic susceptibility from shipboard generated MSCL data, Holes M0066A and M0066B.

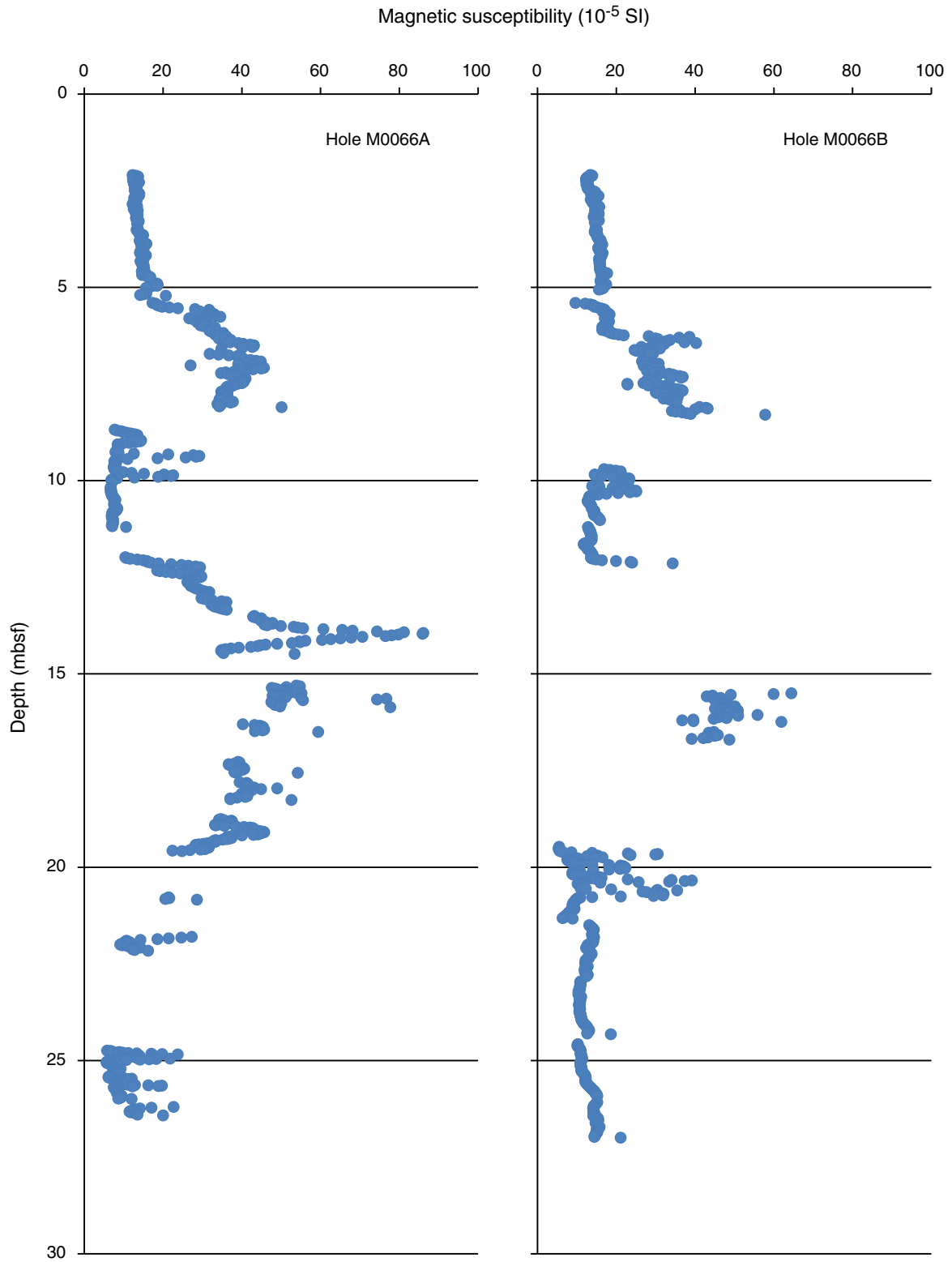




Figure F14. Correlation of the seismic profile with lithostratigraphic boundaries and multisensor core logger magnetic susceptibility data, Site M0066.

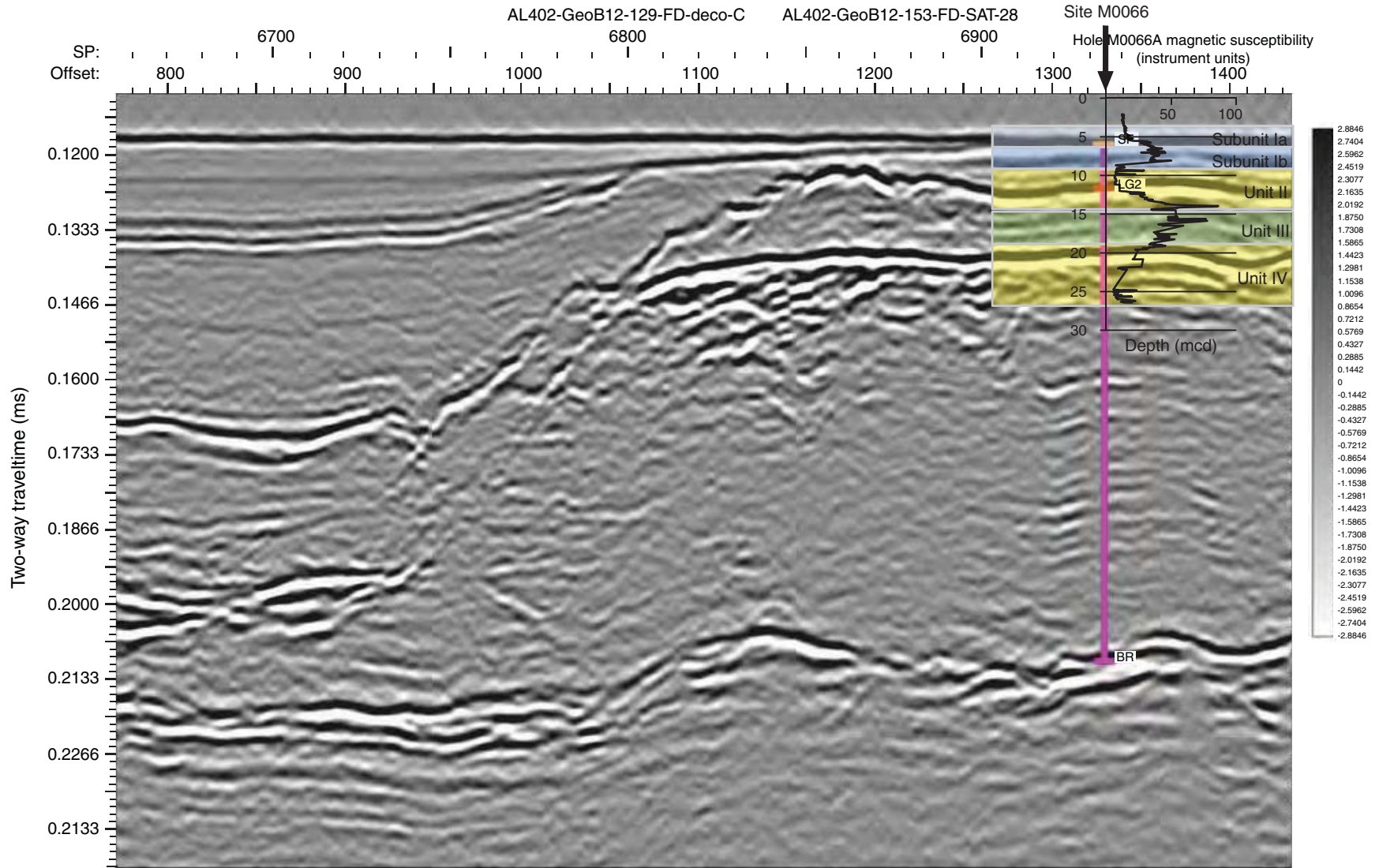




Table T1. Operations, Site M0066. (Continued on next page.)

Core	Coring method	Date (2013)	Time (UTC)	Depth (mbsf)		Recovered (m)	Recovery (%)	Mud type	Comments
				Top	Bottom				
347-M0066A-									
		26 Oct	0723						On site, lowered seabed frame; completed ROV survey for Holes M0066A and M0066B
		26 Oct	0736						Ran pipe
		26 Oct	0816						Relief valve on powerpack sticking again; stopped to fix
		26 Oct	0835						Pipes at seabed frame
1O	NCA	26 Oct	0835	0.00	2.00	0.00	0	Seawater	Open hole first section to avoid possible contamination
2H	PCS	26 Oct	0845	2.00	5.30	3.52	106.67	Seawater	
3H	PCS	26 Oct	0910	5.30	8.60	2.91	88.18	Seawater	Did not push full stroke and only released pressure when string lifted
4H	PCS	26 Oct	1025	8.60	11.35	2.75	100	Guar	Fine sand recovered; piston did not go full stroke
5O	NCA	26 Oct	1110	11.35	11.90	0.00	0	Guar	Washed down remainder of 3.3 m stroke length of piston
6H	PCS	26 Oct	1125	11.90	14.63	2.73	100	Guar	Fine sand recovered; piston did not go full stroke
7O	NCA	26 Oct	1140	14.63	15.20	0.00	0	Guar	Washed down remainder of 3.3 m stroke length of piston
8S	HS	26 Oct	1105	15.20	15.27	0.07	100	Guar	HS run, OSL sample taken; 0.07 m of till recovered; driller did not notice change in drilling, so ~15 mbsf thought to be top of this unit
9N	NRCB	26 Oct	1215	15.20	16.20	0.85	85	Guar	NRCB run started from stop depth of Run 7 without advancing to the recovered length of Run 8 in an attempt to recover clay-like material; very hard diamicton recovered
10N	NRCB	26 Oct	1245	16.20	17.20	0.44	44	Guar	
11N	NRCB	26 Oct	1325	17.20	17.70	0.60	120	Guar	Blocked off, so pulled before 1 m run ended
12N	NRCB	26 Oct	1400	17.70	18.70	0.71	71	Guar	
13N	NRCB	26 Oct	1425	18.70	19.70	1.47	147	Guar	Green sand ~30 cm from base; cored very quickly
14N	NRCB	26 Oct	1445	19.70	20.70	0.27	27	Guar	Gray sand, more silty
15N	NRCB	26 Oct	1510	20.70	21.70	0.30	30	Guar	
16N	NRCB	26 Oct	1530	21.70	22.70	0.70	70	Guar	
17N	NRCB	26 Oct	1610	22.70	23.70	0.00	0	Guar	
18N	NRCB	26 Oct	1510	23.70	24.70	0.05	5	Guar	
19H	PCS	26 Oct	1710	24.70	26.10	3.11	222.14	Guar	3.11 m sand recovered; when washing 3.3 m to the next sample, driller noted lithology change at 26.1 mbsf to a clay-like material; drilling was stopped to take a PCS sample; thought the material recovered was "suck-in" and not depth related, as the PCS did not drop to zero after firing; basal depth of this run is arbitrary
20N	NRCB	26 Oct	1757	26.10	27.00	0.51	56.67	Guar	
21N	NRCB	26 Oct	1815	27.00	28.00	0.31	31	Guar	
		26 Oct	1855						End of hole
		26 Oct	1855						Tripped pipe; lifted template
347-M0066B-									
		26 Oct	1925						On site; lowered seabed frame
		26 Oct	1935						Ran pipe
		26 Oct	1945						Pipes at seabed frame
1O	NCA	26 Oct	1945	0.00	2.00	0.00	0	Seawater	Open hole first section to avoid possible contamination
2H	PCS	26 Oct	1955	2.00	5.30	3.53	106.97	Seawater	
3H	PCS	26 Oct	2040	5.30	8.60	3.14	95.15	Seawater	
4P	PCA	26 Oct	2120	8.60	9.60	0.03	3	Guar	
5H	PCS	26 Oct	2140	9.60	12.90	2.68	81.21	Guar	61 bar
6P	PCA	26 Oct	2205	12.90	13.90	0.05	5	Guar	
7H	PCS	26 Oct	2240	13.90	15.40	3.09	206	Guar	150 bar, pressure did not drop until released; probably sucked core in
8N	NRCB	26 Oct	2320	15.40	16.40	0.90	90	Guar	
9N	NRCB	27 Oct	0002	16.40	17.40	0.34	34	Guar	
10N	NRCB	27 Oct	0040	17.40	18.40	0.02	2	Guar	
11N	NRCB	27 Oct	0110	18.40	19.40	0.00	0	Guar	
12H	PCS	27 Oct	0130	19.40	22.00	2.80	107.69	Guar	
13H	PCS	27 Oct	0205	22.00	25.10	3.14	101.29	Guar	
14H	PCS	27 Oct	0250	25.10	27.85	2.75	100	Guar	70 bar



Table T1 (continued).

Core	Coring method	Date (2013)	Time (UTC)	Depth (mbsf)		Recovered (m)	Recovery (%)	Mud type	Comments
				Top	Bottom				
		27 Oct	0330						End of hole
		27 Oct	0340						Started lifting pipe
		27 Oct	0400						Started washing down pipes that had been through the mudline and also the drill collars and BHA
		27 Oct	0445						Seabed frame pulled up into moonpool; continued washing down with fire hydrant hose to remove contamination
		27 Oct	0515						Seabed frame brought up on deck

HS = hammer sampler, NCA = noncoring assembly, NRCB = nonrotating core barrel, PCA = push coring assembly, PCS = piston coring system. ROV = remotely operated vehicle, OSL = optically stimulated luminescence, BHA = bottom-hole assembly.

Table T2. Interstitial water geochemistry, Site M0066.

Core, section, interval (cm)	Type	Depth (mbsf)	Volume (mL)	Analyte:	pH	Salinity	Alkalinity	Cl ⁻	Br ⁻	SO ₄ ²⁻	H ₂ S	NH ₄ ⁺	Na ⁺	K ⁺	Mg ²⁺	Ca ²⁺	Sr ²⁺	Li ⁺	H ₄ SiO ₄	Ba ²⁺	B	Al	PO ₄ ³⁻	Fe ²⁺	Mn ²⁺	Rb	
				Unit:	ISE	Refraction	meq/L	mM	mM	mM	mM	mM	mM	mM	mM	mM	mM	mM	μM	μM	μM	μM	μM	μM	mM	μM	μM
				Method:			Titration	IC	IC	IC	Photometric	Conductivity	ICP-OES	ICP-OES	ICP-OES	ICP-OES	ICP-OES	ICP-OES	ICP-OES	ICP-OES	ICP-OES	ICP-OES	ICP-OES	ICP-OES	ICP-OES	ICP-OES	ICP-OES
347-M0066A-																											
2H-1, 135-140	Rh	3.38	8		7.82	10.60	—	168.27	0.26	5.79	—	0.14	155.72	2.35	10.25	9.94	37.70	10.73	270.79	0.21	80.38	1.63	0.01	91.65	38.01	0.03	
2H-2, 135-140	Rh	4.88	23		7.62	8.80	4.76	140.16	0.22	3.78	—	0.16	125.40	1.38	7.48	10.13	37.43	10.03	280.36	0.29	59.66	0.48	0.01	123.65	33.61	0.05	
3H-1, 119-124	Rh	6.52	19		7.72	6.60	4.53	103.43	0.17	1.85	—	0.16	94.48	0.96	5.91	9.29	36.51	8.00	431.55	0.66	48.28	1.52	0.01	144.45	21.04	0.08	
3H-2, 136-141	Rh	8.03	39		7.76	5.10	4.69	81.05	0.13	1.08	—	0.14	71.55	0.92	4.47	7.18	31.43	7.35	400.93	1.06	41.90	0.48	0.01	96.28	11.15	0.07	
4H-1, 135-140	Rh	9.98	35		7.89	4.50	3.97	68.58	0.11	1.26	—	0.14	67.73	1.05	4.50	7.68	35.19	6.52	470.71	1.58	49.02	0.82	0.01	93.80	8.73	0.15	
4H-2, 100-105	Rh	11.13	39		8.05	4.90	3.93	74.95	0.12	1.59	—	0.14	67.81	1.10	4.68	6.63	29.30	6.86	287.45	0.90	45.79	0.52	0.01	37.59	9.84	0.20	
6H-1, 135-140	Rh	13.28	38		8.00	3.68	3.76	54.38	0.09	0.77	—	0.12	44.80	0.64	3.70	6.51	32.50	6.34	377.07	1.28	41.90	0.96	0.01	34.54	6.93	0.10	
6H-2, 98-103	Rh	14.41	38		8.33	3.52	3.99	51.49	0.09	0.51	—	0.12	48.19	0.67	4.25	7.87	37.83	6.32	478.90	1.45	48.93	0.93	0.01	50.87	8.35	0.13	
347-M0066B-																											
2H-1, 135-140	Rh	3.38	13		7.91	10.90	4.38	171.03	0.26	6.09	—	0.15	142.19	2.13	10.30	9.75	36.59	10.69	332.42	0.18	85.38	1.52	0.01	103.20	39.54	0.04	
2H-2, 135-140	Rh	4.88	11		7.80	8.74	4.34	134.87	0.21	3.85	—	0.16	124.88	1.26	8.01	10.81	38.37	10.00	326.12	0.29	62.07	1.89	0.01	120.24	36.98	0.02	
3H-1, 135-140	Rh	6.68	40		7.57	6.38	3.93	99.50	0.16	1.89	—	0.16	88.86	0.78	5.61	9.06	34.32	11.42	352.47	0.44	46.43	0.89	0.01	137.95	24.30	0.02	
3H-2, 106-116	Rh	7.91	40		7.70	4.69	4.27	72.99	0.12	0.95	—	0.15	61.20	0.71	3.78	6.68	29.48	10.12	392.74	0.82	38.76	0.00	0.01	75.91	11.42	0.02	
5H-1, 135-140	Rh	10.98	40		7.81	3.38	4.15	46.22	0.08	0.42	—	0.14	35.74	0.55	2.98	5.92	28.52	9.23	427.27	1.23	41.07	1.48	0.01	50.44	6.73	0.11	
5H-2, 93-98	Rh	12.06	40		7.83	3.17	4.10	48.04	0.08	0.58	—	0.14	37.93	0.56	3.14	5.97	28.85	9.14	391.31	1.27	40.05	0.15	0.01	58.57	6.69	0.07	
7H-1, 135-140	Rh	15.28	40		7.83	3.17	3.86	50.25	0.09	0.58	—	0.12	36.52	0.55	3.31	6.59	31.85	10.09	383.12	0.98	38.57	0.82	0.01	39.66	7.22	0.07	
7H-2, 134-140	Rh	16.77	40		7.81	3.43	4.06	53.31	0.09	0.85	—	0.12	40.05	0.51	3.72	6.46	31.39	9.92	340.54	1.17	40.14	0.00	0.01	25.55	7.06	0.06	
12H-1, 135-140	Rh	20.78	40		7.78	1.75	4.16	25.00	0.05	0.19	—	0.06	15.15	0.38	2.16	4.91	25.50	10.94	451.13	1.75	45.97	2.15	0.01	27.67	6.17	0.14	
13H-1, 135-140	Rh	22.78	40		7.78	2.11	3.76	30.51	0.06	0.52	—	0.06	18.02	0.39	2.59	5.63	28.71	11.34	439.02	2.05	46.62	0.26	0.01	29.58	5.37	0.12	
14H-1, 133-138	Rh	25.86	40		7.87	1.85	3.80	27.30	0.05	0.28	—	0.06	17.64	0.44	2.26	5.16	27.88	11.25	436.18	1.81	44.68	0.00	0.01	13.61	5.09	0.20	
Reference samples																											
R2 salt brine mud 1	—	—	—		7.45	170.07	2.35	3448.94	0.00	17.47	0.00	0.00	3372.77	5.85	14.36	12.48	420.57	6.06	35.78	8.98	137.36	0.22	0.01	13.54	6.46	0.07	
R3 seawater from mud pump	—	—	—		7.69	16.87	2.14	265.91	0.33	11.68	0.00	0.00	254.37	4.99	23.53	5.07	45.41	11.86	7.62	3.18	187.77	0.56	0.01	0.00	2.87	0.06	
R4 grease 1 drill pipe	—	—	—		6.28	2.56	0.26	0.18	0.00	0.01	0.00	0.02	0.00	0.00	0.00	0.01	0.13	1.18	0.57	4.69	8.69	0.00	0.01	0.00	2.86	0.00	
R5 grease 2 pipes	—	—	—		6.51	3.04	0.27	0.09	0.00	0.00	0.00	0.02	0.00	0.00	0.00	0.04	0.08	0.29	0.00	4.05	6.94	0.00	0.01	0.00	2.86	0.00	
R6 grease 3 core barrel	—	—	—		6.54	4.49	0.26	0.08	0.00	0.00	0.00	0.03	0.00	0.00	0.00	0.03	0.07	0.29	1.53	3.90	6.47	0.00	0.01	0.00	2.86	0.00	
R7 grease 4 'moly' piston rod grease	—	—	—		4.34	0.00	0.11	0.05	0.00	0.00	0.00	0.00	0.00	0.00	0.00	0.01	0.01	0.41	0.00	0.43	5.09	0.00	0.01	0.00	2.86	0.00	
R8 grease 5 pipe thread	—	—	—		6.30	5.56	0.23	0.39	0.00	0.03	0.00	0.03	0.00	0.00	0.00	0.00	0.05	1.57	0.61	3.01	6.94	0.00	0.01	0.00	2.86	0.00	
R9 tap water GC	—	—	—		6.49	0.00	0.26	5.06	0.01	0.04	0.00	0.00	4.65	0.14	0.05	0.03	0.24	0.90	7.23	8.71	104.80	0.22	0.01	0.00	2.89	0.03	
R10 H ₂ O _d ELGA	—	—	—		6.21	0.00	0.35	0.06	0.00	0.00	0.00	0.00	0.00	0.00	0.00	0.01	0.38	0.38	0.53	1.30	9.99	0.37	0.01	0.00	2.86	0.00	
R11 mud 2 (GSS50)	—	—	—		7.74	41.48	9.62	643.71	0.49	20.60	0.00	1.36	807.31	9.05	41.80	8.83	98.60	19.35	23.11	1.69	343.63	1.63	0.01	8.99	5.15	0.10	
R12 mud 3 (guar gum)	—	—	—		6.40	16.60	2.20	239.64	0.36	12.35	0.00	0.07	223.23	5.61	24.40	4.91	36.57	12.51	8.47	1.94	192.03	0.37	0.01	0.00	3.02	0.05	
R13 seawater/drill water	—	—	—		7.83	14.94	2.21	241.08	0.36	8.87	0.00	0.00	216.62	5.09	24.56	4.96	37.02	12.67	5.70	1.88	190.27	0.00	0.01	0.56	2.93	0.06	
R26 M0064/surface seawater	—	—	—		7.76	6.54	1.85	113.81	0.17	5.96	0.00	0.00	103.57	2.36	11.62	2.79	18.63	5.17	6.94	0.02	88.34	0.15	0.01	0.00	2.87	0.02	

Rh = Rhizon sample. ISE = ion-specific electrode, IC = ion chromatography, ICP-OES = inductively coupled plasma-optical emission spectroscopy. — = no data reported for samples with insufficient pore water volumes.



Table T3. Calculated salinity and elemental ratios of interstitial waters, Site M0066.

Core, section, interval (cm)	Type	Depth (mbsf)	Cl ⁻ based salinity	Na/Cl (mM/mM)	Ca/Cl (mM/mM)	Mg/Cl (mM/mM)	K/Cl (mM/mM)	Br/Cl (μM/mM)	B/Cl (μM/mM)
347-M0066A-									
2H-1, 135–140	Rh	3.38	10.55	0.93	0.06	0.06	0.01	1.53	0.48
2H-2, 135–140	Rh	4.88	8.79	0.89	0.07	0.05	0.01	1.57	0.43
3H-1, 119–124	Rh	6.52	6.49	0.91	0.09	0.06	0.01	1.63	0.47
3H-2, 136–141	Rh	8.03	5.08	0.88	0.09	0.06	0.01	1.66	0.52
4H-1, 135–140	Rh	9.98	4.30	0.99	0.11	0.07	0.02	1.62	0.71
4H-2, 100–105	Rh	11.13	4.70	0.90	0.09	0.06	0.01	1.59	0.61
6H-1, 135–140	Rh	13.28	3.41	0.82	0.12	0.07	0.01	1.69	0.77
6H-2, 98–103	Rh	14.41	3.23	0.94	0.15	0.08	0.01	1.73	0.95
347-M0066B-									
2H-1, 135–140	Rh	3.38	10.73	0.83	0.06	0.06	0.01	1.54	0.50
2H-2, 135–140	Rh	4.88	8.46	0.93	0.08	0.06	0.01	1.57	0.46
3H-1, 135–140	Rh	6.68	6.24	0.89	0.09	0.06	0.01	1.63	0.47
3H-2, 106–116	Rh	7.91	4.58	0.84	0.09	0.05	0.01	1.62	0.53
5H-1, 135–140	Rh	10.98	2.90	0.77	0.13	0.06	0.01	1.74	0.89
5H-2, 93–98	Rh	12.06	3.01	0.79	0.12	0.07	0.01	1.73	0.83
7H-1, 135–140	Rh	15.28	3.15	0.73	0.13	0.07	0.01	1.73	0.77
7H-2, 134–140	Rh	16.77	3.34	0.75	0.12	0.07	0.01	1.69	0.75
12H-1, 135–140	Rh	20.78	1.57	0.61	0.20	0.09	0.02	1.97	1.84
13H-1, 135–140	Rh	22.78	1.91	0.59	0.18	0.08	0.01	1.86	1.53
14H-1, 133–138	Rh	25.86	1.71	0.65	0.19	0.08	0.02	1.93	1.64

Rh = Rhizon sample.

Table T4. Total carbon (TC), total organic carbon (TOC), total inorganic carbon (TIC), and total sulfur (TS) in sediment, Site M0066.

Core, section, interval (cm)	Depth (mbsf)	TC (wt%)	TOC (wt%)	TIC (wt%)	TS (wt%)
347-M0066A-					
2H-1, 42–43	2.42	1.85	0.54	1.30	0.14
2H-2, 145–146	4.95	1.54	0.45	1.09	0.12
3H-1, 121.5–122.5	6.52	3.08	0.13	2.95	0.31
4H-2, 20–21	10.30	0.87	0.00	0.86	0.14
6H-1, 82–83	12.72	1.23	0.01	1.22	0.24
9H-1, 15–16	15.35	2.33	0.11	2.21	0.28
10H-1, 13–14	16.33	3.00	0.16	2.84	0.32
11H-1, 13–14	17.33	2.72	0.28	2.44	0.51
12H-1, 24–25	17.94	3.04	0.27	2.77	0.58
13H-1, 33–34	19.03	3.21	0.21	3.00	0.67
15H-1, 9.5–10.5	20.80	2.14	0.20	1.93	0.40
16H-1, 20–21	21.90	1.38	0.09	1.29	0.27
19H-2, 80–81	27.00	0.67	0.04	0.63	0.19
20H-1, 27–28	26.37	1.26	0.06	1.20	0.30
347-M0066B-					
2H-1, 90–91	2.90	2.06	0.55	1.51	0.15
3H-1, 44–45	5.74	2.13	0.50	1.63	0.15
5H-1, 101–102	10.61	1.73	0.03	1.70	0.24
7H-2, 61–62	16.01	1.28	0.05	1.23	0.17
8H-1, 32–33	15.72	2.64	0.14	2.50	0.31
12H-2, 18–19	21.08	2.95	0.16	2.80	0.60
12H-2, 110–111	22.00	0.57	0.04	0.53	0.23
13H-1, 63–64	22.03	2.15	0.12	2.03	0.40
14H-1, 77–78	25.27	0.97	0.05	0.92	0.29

Table T5. Composite depth scale, Site M0066.

Core	Offset (m)	Top depth	
		(mbsf)	(mcd)
347-M0066A-			
2H	0.30	2.0	2.30
3H	0.83	5.3	6.13
4H	0.83	8.6	9.43
6H	0.83	11.9	12.73
9N	0.83	15.2	16.03
10N	0.83	16.2	17.03
11N	0.83	17.2	18.03
12N	0.83	17.7	18.53
13N	0.83	18.7	19.53
14N	0.83	19.7	20.53
15N	0.83	20.7	21.53
16N	0.83	21.7	22.53
18N	0.83	23.7	24.53
19H	0.83	24.7	25.53
20N	0.83	26.1	26.93
347-M0066B-			
2H	0.00	2.0	2.00
3H	0.00	5.3	5.30
5H	0.47	9.6	10.07
6P	0.47	12.9	13.37
7H	-1.73	13.9	12.17
8N	0.47	15.4	15.87
9N	0.47	16.4	16.87
10N	0.47	17.4	17.87
12H	0.47	19.4	19.87
13H	0.47	21.4	21.87
14H	0.47	24.5	24.97

Table T6. Splice tie points, Site M0066.

Hole, core section, interval (cm)	Depth (mbsf)	Depth (mcd)		Hole, core section, interval (cm)
347-				347-
M0066B-2H-3, 27	5.40	5.40	Append	M0066B-3H-1, 10
M0066B-3H-1, 113	5.60	6.44	Tie to	M0066A-3H-1, 30
M0066A-3H-2, 145	8.68	9.51	Append	M0066A-4H-1, 8
M0066A-4H-1, 117	10.15	10.61	Tie to	M0066B-5H-1, 54
M0066B-5H-2, 88	12.08	12.45	Tie to	M0066A-6H-1, 18

Table T7. Sound velocity data for lithostratigraphic units, Site M0066.

Unit	Thickness of unit (m)	Sound velocity (m/s)*	TWT (ms)	Depth (m)	Depth (mbsf)
Seafloor	82	1475	0.1112	82	0
Ia	4.98	1582	0.1175	86.98	4.98
Ib	3.62	1582	0.1221	90.6	8.6
II	6.6	1582	0.1304	97.2	15.2
III	4.31	1780	0.1352	101.51	19.51
IV	7.8	1478	0.1458	109.31	27.31

* = sound velocities are based on values measured during the OSP. TWT = two-way travelttime.